Pergamon

PII: S0191-8141(97)00026-6

Journal of Structural Geology, Vol. 19, No. 8, pp. 1121 to 1135, 1997

0191-8141/97 $17.00 + 0.00

Crenulation cleavage formation: Evolving diffusion, deformation and equilibration mechanisms with increasing metamorphic grade

BRENTON WORLEY, ROGER POWELL and CHRISTOPHER J. L. WILSON

School of Earth Sciences, The University of Melbourne, Parkville, Victoria 3052, Australia

(*Received* 12 *July* 1996; *accepted in revised form* 13 *May* 1997)

Abstract—An integrated microstructural and chemical study of crenulation cleavages developed in chlorite- to garnet-zone schists from the Wenchuan-Maowen shear zone, central China, has resulted in the recognition of the deformation and equilibration mechanisms operating during their formation at a range of temperatures. Deformation during crenulation cleavage formation at chlorite- to biotite-zone temperatures (~520°C) is essentially a solution-deposition process, in which transport occurred by a combination of localized advection and grain-boundary diffusion. Recrystallization and hence equilibration of muscovite in discrete cleavages is recognized by distinct compositional differences between muscovite from different domains. Crenulation cleavages developed in garnet-zone schist are characterized by homogeneous muscovite compositions across domains and microstructures related to intracrystalline deformation, indicating an increasing importance of volume diffusion and diffusive equilibration of mica at temperatures greater than ~520°C. © 1997 Elsevier Science Ltd.

INTRODUCTION

Metamorphic differentiation and cleavage development associated with the crenulation of a pre-existing fabric are extremely common in layer silicate-bearing medium- to low-grade metamorphic rocks (Cosgrove, 1976; Gray, 1979). They are generally related to a combination of mechanical grain rotations, in response to microfolding, and mass transfer processes such as pressure solution and recrystallization involving a grain-boundary fluid. There are two main schools of thought on the scale and, hence, the driving force of transport during such mass transfer processes. For chemical-potential-driven processes, transport distances are small (Cosgrove, 1976; Gray, 1977, 1979; Gray and Durney, 1979; Waldron and Sandiford, 1988). Such processes can only be applicable on a scale of a single grain or possibly of small microfolds, and hence the system may be considered as 'closed' on a hand-specimen scale. In contrast, fluid flow processes can operate on a much larger scale (Etheridge *et al.*, 1983), in which case transport distances can be considerable and the system is essentially 'open' on a hand-specimen scale.

Recrystallization of mica in the cleavage domains is another significant component in the deformation process. Although recognizing the strong preferred orientation of muscovite in cleavage domains, Gray (1979) attributes this alignment to mechanical rotation of the pre-existing grains coupled with quartz removal via chemical-potential-driven pressure solution. Marlow and Etheridge (1977), however, propose that muscovite within cleavage domains had nucleated and grown with an orientation and shape controlled by features such as microstructural anisotropies and the stress and/or strain history of the domain.

A few studies indicate that, at upper greenschist to lower amphibolite facies conditions, dislocation creep and other crystal plastic deformation processes dominate the formation of crenulation cleavages (Bell and Rubenach, 1983) and schistose fabrics (Vernon, 1977; Wilson and Bell, 1979). With increasing metamorphic grade, quartz deformation is dominated by grain-boundary migration recrystallization (Wilson, 1973). However, somewhat surprisingly, there is a lack of geological literature dealing with the evolution of crenulation cleavage morphology and deformation mechanisms with increasing temperature.

DIFFUSION, DEFORMATION AND EQUILIBRATION

Deformation and metamorphism of a mineral aggregate, of which the formation of a crenulation cleavage is one example, involves contributions from a number of processes responsible for the redistribution of material within individual minerals and the mineral aggregate as a whole. Therefore, to understand the controls on crenulation cleavage formation, it is necessary to consider these processes and how their relative contributions vary with changing conditions, in particular temperature. It is necessary to evaluate the contribution of the following.

(1) *Mechanical rotation of grains.*

(2) *Provision/removal of material from grain boundaries.* Two main methods are involved:

(a) grain-boundary diffusion—where movement of material along grain boundaries occurs in response to chemical potential gradients in either a fluid-absent environment or through a static grain-boundary fluid;

(b) advection—involves the transport of material by a moving fluid, presumably mainly buoyancy-driven.The main difference between the two processes is whether the fluid is stationary or mobile, the consequence being that

advection can operate on a much larger scale than grain-boundary diffusion (e.g. Etheridge *et al.*, 1983). However, strictly speaking, whenever a grain-boundary fluid is moving, even if on only a μm to mm scale, the process should be thought of, and treated in terms of, advection rather than grain-boundary diffusion.

(3) *Chemical changes within the grains.* As temperature and pressure vary during metamorphism, mineral compositions also change to try to maintain thermodynamic equilibrium. There are two main processes by which mineral equilibration can be achieved:

(a) recrystallization (or nucleation and growth of a new phase);

(b) volume diffusion.

All of the above processes are involved in deformation and metamorphism, but when investigating crenulation cleavage formation, workers have tended to concentrate on the first two groups, mechanical rotation of grains accompanied by material transport (e.g. Cosgrove, 1976; Gray, 1977, 1979; Gray and Durney, 1979). However, all three groups are likely to be involved in the overall deformation process, and the role of the last group, in addition to being central to the equilibration of minerals and mineral assemblages, may be assessed by specifically looking at mineral composition variations.

Equilibration of minerals can be achieved by intracrystalline volume diffusion, or recrystallization and mineral growth. Material transport to or away from the mineral during these processes may take place by either grain-boundary diffusion or advective fluid flow. However, both modes of transport will have essentially the same overall effect of supplying material to the mineral grain boundaries. Temperature is likely to be the controlling factor which determines whether equilibration can occur by volume diffusion, or if recrystallization is necessary to change mineral compositions. To illustrate this it is helpful to consider the thermal dependence of diffusion. In general the coefficient of diffusion (D) is exponentially related to $1/T$ following the Arrhenius relationship which is typical of thermally activated processes:

$$D = D_0 e^{-Q/RT}, \quad (1)$$

where D_0 is the pre-exponential factor, which is D at infinitely high temperature, R is the gas constant, T is temperature and Q is the activation energy. As the activation energy for volume diffusion (Q_v) is much larger than the activation energy for grain-boundary diffusion (Q_{gb}) (Vernon, 1976; Putnis, 1992), grain-boundary diffusion is easier than volume diffusion, with the latter negligible at low temperatures. With increasing temperature the rate of volume diffusion increases, until diffusion through the mineral lattice can occur at geologically significant rates. Therefore, at suitably high temperatures, equilibration of minerals will occur as elements are able to diffuse through minerals. In comparison, at low temperatures, the insignificant rate of volume diffusion necessitates recrystallization of mineral grains to achieve equilibration, i.e. 'crystallization equilibration'. In the context of this generalization the activation energy Q (and D_0) are different for different diffusing elements and, particularly for volume diffusion, vary between minerals. In additional, diffusion rates are grain size dependent. However, for a given mineral grain, and specifically for a particular element, temperature is the factor which controls whether volume diffusion will be a significant process. A common and probably one of the best understood geological examples of the control of grain-boundary vs volume diffusion on mineral equilibration is the difference in zoning patterns in garnets which have undergone greenschist or lower amphibolite vs upper amphibolite or granulite facies metamorphism.

Considering the overall deformation mechanism, processes such as pressure solution involve transport of material by grain-boundary diffusion or advection with associated recrystallization/crystallization of minerals. Equilibration is controlled by crystallization, if it occurs. Conversely, intracrystalline crystal–plastic deformation depends on significant volume diffusion to enable the movement of dislocations through the crystal structure and the important equilibration mechanism will be diffusive equilibration. As equilibration involves a change in the chemical composition of specific mineral phases it may be possible to determine the dominant equilibration mechanism by a detailed study of mineral chemistry and, by relating this to microstructural observations, assess the relative contributions of deformation mechanisms during deformation. This approach is taken in this integrated microstructural and chemical investigation of crenulation cleavages developed in chlorite- to garnet-zone schists from the Wenchuan-Mouwen shear zone, central China.

GEOLOGICAL FRAMEWORK AND SAMPLE SELECTION

Roughly coinciding with the eastern edge of the Tibetan Plateau in China (Fig. 1a), the Wenchuan-Maowen shear zone is a 20–25 km wide zone of non-coaxial shear which developed along the margin between the mobile Songpan-Garzê Fold Belt and stable Yangtze Craton during the Late Triassic Indosinian orogeny (Chen *et al.*, 1995; Worley and Wilson, 1996). The Songpan-Garzê Fold Belt is composed of predominantly deep-water Palaeozoic–Mesozoic sedimentary rocks resting on crystalline Proterozoic basement rocks. During the Indosinian orogeny this sequence experienced three principal phases of ductile deformation (D_1–D_{3p} of Worley and Wilson, 1996), lower greenschist to amphibolite facies 'Barrovian-type' regional metamorphism and extensive granite magmatism. The second and third phases of deformation were strongly partitioned into the Wenchuan-Maowen shear zone where peak meta-

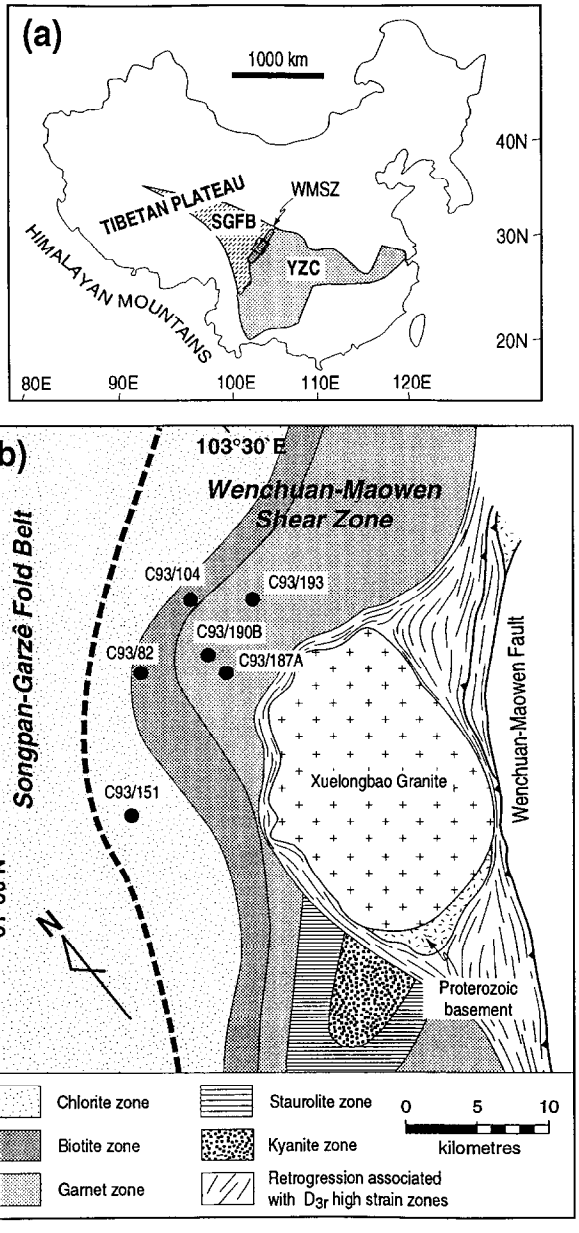

Fig. 1. (a) Locality map of China indicating the position of the Wenchuan-Mouwen shear zone (WMSZ) relative to the Songpan-Ganzê Fold Belt (SGFB) and Yangtze Craton (YZC). (b) Simplified structural–metamorphic map of the Wenchuan-Maowen shear zone illustrating sample locations relative to the metamorphic isograds and some of the major structural features.

morphic conditions reached the kyanite zone of the amphibolite facies during D_{3p} (Fig. 1b) (Worley and Wilson, 1996). The first phase of deformation (D_1) affected the whole Songpan-Garzê Fold Belt and was responsible for the formation of a pervasive slaty cleavage parallel to the axial surface of isoclinal F_1 folds. Within the Wenchuan-Maowen shear zone and other areas of localized high strain, this slaty cleavage was crenulated during D_2. The resulting crenulation cleavage (S_2), which parallels the axial surface of F_2 folds, increases in intensity, with increasing D_2 strain and metamorphic grade from west to east across the shear zone. The gradual increase in strain across the shear zone is also indicated by the sinistral rotation and eventual transposition of the D_1 structural elements, and the tightening of F_2 folds in conjunction with their developing consistent sinistral asymmetry. At a mesoscopic scale this strain increase results in the evolution of the S_2 fabric from a spaced crenulation cleavage to a domainal crenulation cleavage and finally a pervasive schistosity, which is equivalent to a complete schistosity cycle of Bell and Rubenach (1983). Microscopically, similar variations in the morphology of the S_2 fabric can be attributed to local strain partitioning within single samples (Worley and Wilson, 1996). The S_2 fabric in the eastern portion of the Wenchuan-Maowen shear zone was variably crenulated or reactivated during essentially coplanar D_{3p} reverse shear (Chen *et al.*, 1995; Worley and Wilson, 1996). Localized reverse shear (D_{3r}) during uplift of the fold belt resulted in large-scale reactivation and retrogression of the eastern Wenchuan-Maowen shear zone.

More than 100 samples collected from across the Wenchuan-Maowen shear zone were examined microscopically to determine the nature of the S_2 fabric and the relationship between increasing metamorphic grade, strain and cleavage morphology. Although sediment lithologies within the shear zone include limestone and a continuous range from psammite to pelite, the samples used in this study were restricted to pelitic and psammopelitic lithologies, with most observations from mica-rich layers. Data from six representative samples (Fig. 1b), one from the chlorite zone, two from the biotite zone and three from the garnet zone, are presented here as these best illustrate the evolution of the crenulation cleavage. All microstructural observations and photographs presented in this paper are from sections cut normal to the axes of the microcrenulation and minor F_2 folds.

CRENULATION CLEAVAGE MORPHOLOGY

Throughout the following discussions the crenulation cleavages are described in terms of P- and Q-domains, which refer to phyllosilicate- and quartz-rich domains, respectively (Marlow and Etheridge, 1977; Stephens *et al.*, 1979). We have used the classification system of Gray (1977) which defines crenulation cleavage end-members on the basis of morphological characteristics.

Discrete: "The cleavage has sharp, distinct boundaries which truncate the initial fabric".

Zonal: "The cleavage is a zone and has diffuse somewhat arbitrary boundaries through which the initial fabric is continuous".

Gray also recognized that these two cleavage varieties may be gradational into one another and suggested that discrete crenulation cleavages develop from the zonal types (Gray, 1977; Gray and Durney, 1979).

Chlorite zone

Fine-grained chlorite-zone schist collected approximately 300 m from the biotite isograd contains a pervasive slaty cleavage (S_1), defined by a grain-shape alignment of muscovite and chlorite subparallel to alternating quartz + albite-rich and foliated muscovite + chlorite-rich layers which represent bedding. Uncrenulated muscovite + chlorite-rich layers and Q-domains are composed of muscovite + chlorite ($\sim 5 \times 20 \mu m$) and quartz + albite ($\sim 20 \times 40 \mu m$) with accessory tourmaline + rutile and rarely minor graphite. The S_2 crenulation cleavage is prominent but generally restricted to muscovite + chlorite-rich regions adjacent to the quartz-rich layers, and appears to be spatially related to small F_2 folds/buckles in these layers. These crenulations are consistent with a Type-B instability of Gray (1977) where the crenulation cleavage initially develops in response to strain perturbations associated with the buckling of an isolated competent layer (i.e. the quartz-rich layer in Fig. 2a). The cleavage is most prominent in the short limbs of the buckle folds where the quartz-rich layers are truncated and offset along discrete cleavage zones. The quartz-rich layer in Fig. 2(a) has also undergone extensive thinning in the cleavage-affected short limb, and maintains a relatively constant thickness throughout the hinge zones and long limbs. Quartz grains in the quartz-rich layer are generally equant and approximately 30–50 μm in size. Grain boundaries are relatively regular, and there is minor formation of subgrains and undulose extinction. However, no increase in the intensity of these intracrystalline deformation features occurs as P-domain boundaries are approached. Instead the quartz grains are truncated by the discrete cleavage P-domains. The P-domains of the discrete cleavages are generally thin, 15–25 μm (Fig. 2a & b), and composed of muscovite ($\sim 5 \times 20 \mu m$ grain size) + graphite + rutile $\pm$ tourmaline. Muscovite in the P-domains shows a strong alignment, with the (001) planes parallel, within 5–10°, to the domain boundaries. The S_1 cleavage is variably crenulated in the Q-domains and abuts the P-domains of the discrete crenulation cleavage at a variety of angles from ~ 30 to 90° (Fig. 2b).

The crenulation cleavage morphology changes longitudinally away from the folded quartz-rich layers from discrete to zonal within individual cleavage domains (Fig. 2c & d). The composition of the P-domains varies synchronously with the morphological change, predominantly via a decrease in the graphite content. The resulting assemblage of muscovite $\pm$ rutile $\pm$ tourmaline still lacks quartz and chlorite. P-domains of zonal cleavages are coincident with the limbs of microfolds (Fig. 2c & d), and the Q-domains represent the hinge zones of these folds. The change in orientation of muscovite grains is gradational from the Q- into the P-domains where the (001) cleavage traces are essentially parallel to the domain boundaries (and axial surface of the microfolds).

Biotite zone

Biotite–muscovite schist in the lower biotite zone (Fig. 1b) has an S_1 slaty cleavage which is again defined by a marked grain-shape orientation parallel to alternating quartz and muscovite + chlorite layers representing bedding. The S_2 crenulation cleavage is penetratively developed throughout all but the most quartz-rich layers, but the morphology varies markedly with mica content. Thick ($\sim 100 \mu m$) zonal and discrete cleavages (Fig. 2e–f, Fig. 3a) are ubiquitous in mica-rich regions with assemblages of muscovite $\pm$ ilmenite $\pm$ tourmaline $\pm$ graphite and muscovite + chlorite + quartz + plagioclase (An_{15}) $\pm$ ilmenite $\pm$ tourmaline in P- and Q-domains, respectively. In the relatively 'mica-poor' layers the crenulation cleavage is predominantly a discrete cleavage with thin (20–40 μm) P-domains composed of muscovite ($\sim 5 \times 30 \mu m$) $\pm$ ilmenite $\pm$ tourmaline $\pm$ biotite. Q-domains are composed of muscovite + chlorite ($\sim 10 \times 50 \mu m$) + quartz (up to $50 \times 75 \mu m$) + plagioclase + ilmenite $\pm$ tourmaline, as well as biotite porphyroblasts (up to 1 mm) which overgrow a slightly crenulated S_1 fabric but are strongly wrapped by S_2 P-domains rather than overgrowing them (Fig. 2e). No evidence of intracrystalline deformation is observed in either the biotite porphyroblasts or quartz grains from the Q-domains. However, relatively equant quartz grains (100–200 μm) within quartz-rich layers show some development of subgrains and undulose extinction.

Biotite–muscovite schist within the upper biotite zone exhibits a bedding-parallel S_1 slaty cleavage which is folded and cut by a prominent S_2 crenulation cleavage. The crenulation cleavage is defined by generally discrete P- and Q-domains. P-domains are composed of muscovite ($\sim 20 \times 75 \mu m$) and/or biotite (up to 500 μm) with minor ilmenite, graphite and tourmaline (Figs 2f and 3a). Muscovite in the centre of the P-domains is aligned with (001) parallel to the overall cleavage orientation. The muscovite grains at the edge of the P-domains (Fig. 3a) are at a slight angle to the boundary, but are distinctly discordant to the neighbouring grains in the Q-domains. Elongate biotite porphyroblasts, predominantly aligned parallel to the cleavage, are present in both the P-domains, where they are commonly the major cleavage-forming mineral (Fig. 2f), and the Q-domains, where they overgrow the crenulated S_1 fabric (Fig. 3b). There, the S_1 fabric is defined by a grain-shape orientation of muscovite + chlorite ($\sim 20 \times 100 \mu m$) and quartz + plagioclase (An_{25}) (100–200 μm) + ilmenite + tourmaline. Rare biotite porphyroblasts, which are distinctly discordant to both the S_1 and S_2 fabrics (Figs 2f and 3c), contain inclusion trails parallel to the S_2 cleavage domains indicating post-cleavage growth. Neither, the post- nor the syn-cleavage biotite porphyroblasts exhibit any kinking or other evidence of intracrystalline deformation. However, quartz and plagioclase occasionally exhibit undulose extinction and subgrain formation especially in the quartz-rich layers. Although there is no

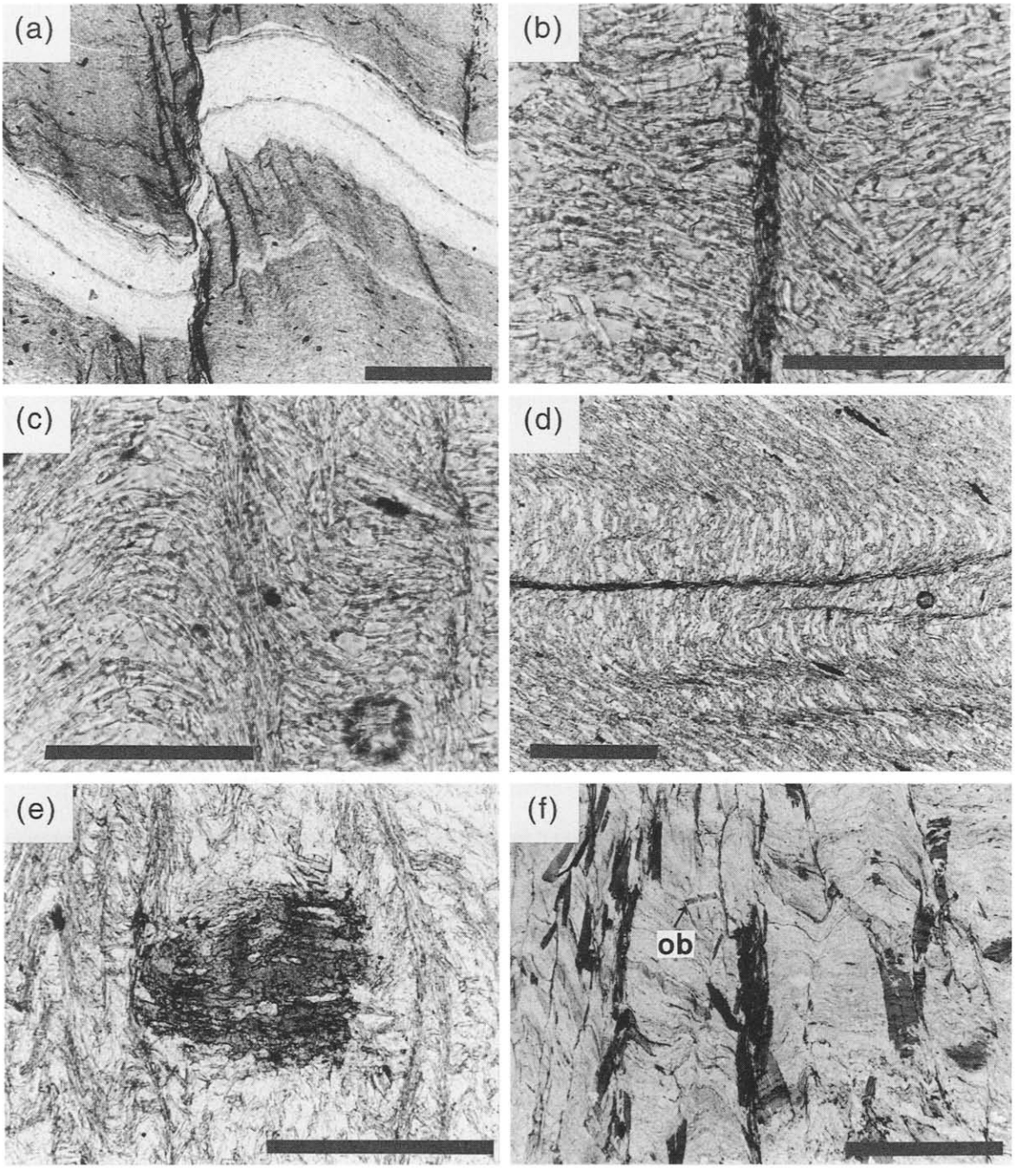

Fig. 2. Cleavage morphology at chlorite-zone (a–d) and biotite-zone (e & f) conditions. (a) Discrete crenulation cleavage associated with F_2 folding of quartz-rich layer. The short limb of the fold has undergone extensive thinning and is truncated by the discrete cleavage. Note the variation in cleavage morphologies in the mica-rich layers. Scale bar = 1 mm. (b)–(d) are close-ups of the same sample as (a). (b) Single P-domain of discrete crenulation cleavage in mica-rich layer. Scale bar = 100 μm. (c) Zonal crenulation cleavage in mica-rich layer. Note that the P-domain of the cleavage is developed along the limbs of microfolds. Scale bar = 100 μm. (d) Evolution of the cleavage morphology from discrete to zonal along a single cleavage domain. Scale bar = 250 μm. (e) Discrete crenulation cleavages and biotite porphyroblast in relatively 'mica-poor' layer. The biotite porphyroblast, which is within an S_2 Q-domain, has preserved the S_1 fabric as inclusion trails and is wrapped by S_2 P-domains. Scale bar = 500 μm. (f) Predominantly discrete crenulation cleavage commonly defined by elongate biotite porphyroblasts in the upper biotite zone. Local post-cleavage biotite porphyroblasts (ob) are oblique to the cleavage domains. Scale bar = 2 mm.

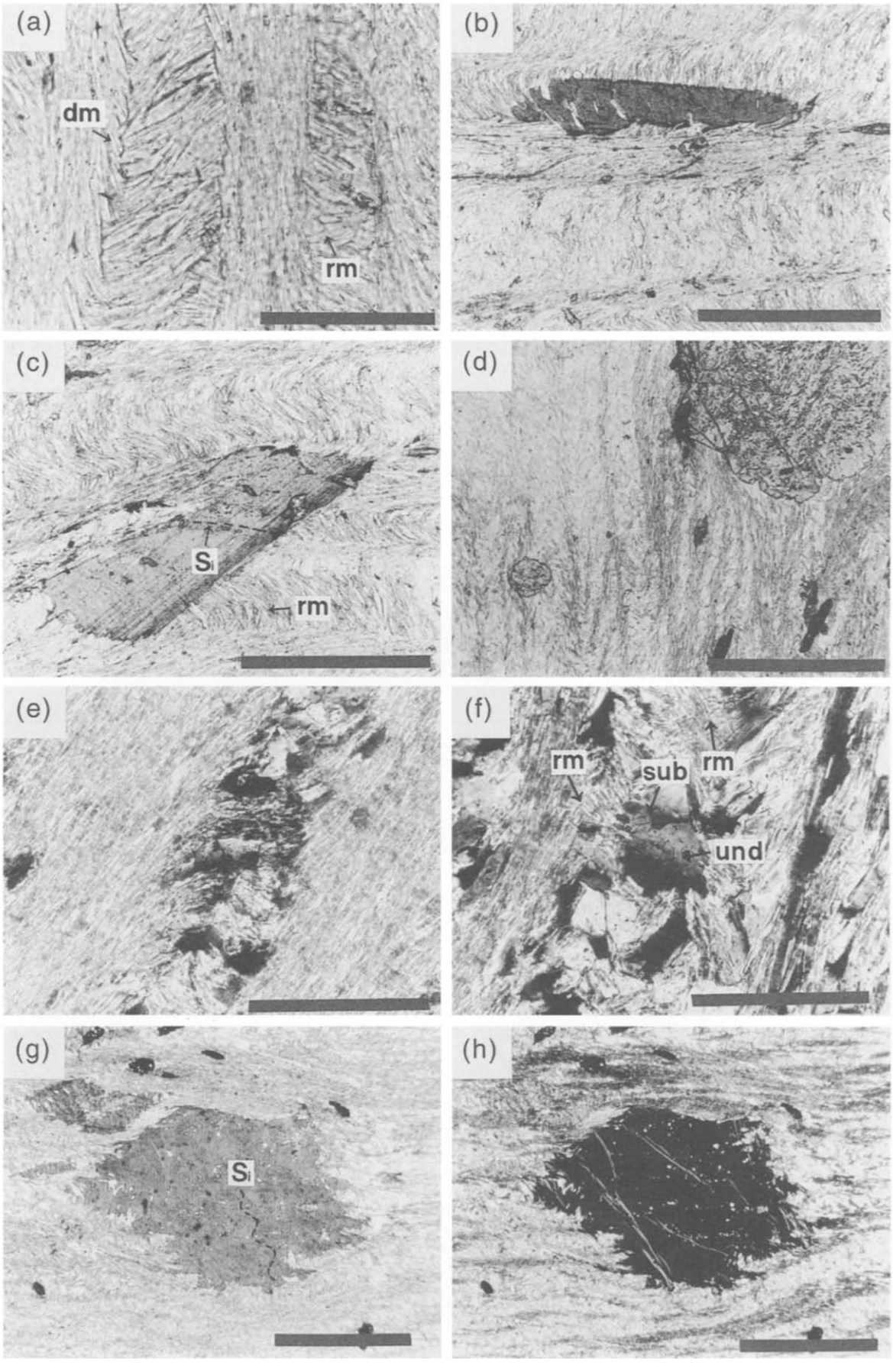
(a)
dm
rm
(b)
(c)
Si
rm
(d)
(e)
(f)
rm
sub
rm
und
(g)
Si
(h)

evidence of kinking in muscovite, it is commonly reoriented around microfolds with neighbouring grains at oblique angles to each other (Fig. 3a & c).

Garnet zone

Bedding and the S_1 cleavage have generally been folded into tight to isoclinal mesoscopic F_2 folds in garnet–biotite schists from the garnet zone. The morphology of the associated S_2 fabric varies within mica-rich layers from a zonal (Fig. 3d & e) to a discrete (Fig. 3d & f) crenulation cleavage through to a penetrative schistosity (Fig. 3d), with increasing mica content. The variations are the result of local strain partitioning around small-scale (wavelength <5 cm) F_2 folds and garnet and biotite porphyroblasts. In both zonal and discrete crenulation cleavages the P-domains are composed of muscovite ($\sim 30 \times 100$ μm) $\pm$ ilmenite $\pm$ tourmaline, whereas Q-domains contain the assemblage muscovite + chlorite ($\sim 30 \times 100$ μm) + quartz $\pm$ plagioclase (An_{25-30}) ($>100\mu$m) $\pm$ ilmenite $\pm$ tourmaline. Numerous garnet and biotite porphyroblasts overgrow the crenulation cleavage, preserving crenulated inclusion trails (Fig. 3d & g) and layers of quartz inclusions parallel to S_2 which probably represent overgrown Q-domains (Fig. 3g). The S_2 fabric is commonly wrapped around these porphyroblasts and many of the biotite porphyroblasts are extensively kinked (Fig. 3h). The hinge zones of microcrenulations are preserved in Q-domains of both zonal (Fig. 3e) and discrete (Fig. 3f) crenulation cleavages. In zonal cleavage Q-domains the crenulations are open, often asymmetric, and muscovite, chlorite and quartz grains exhibit partial rotation into the P-domains. Quartz in the Q-domains exhibits undulose extinction, and subgrains are common with muscovite and chlorite exhibiting gentle undulose extinction. At the margins of the P-domains, quartz and muscovite are elongate and oriented at a small angle to the trace of the cleavage (Fig. 3e). Muscovite in the centre of the P-domains is parallel to the overall cleavage orientation. Crenulations preserved in Q-domains of discrete cleavages are tight, and the muscovite and chlorite grains, which exhibit slight undulose extinction, are generally highly misoriented with respect to each other around the crenulation hinges (Fig. 3f), but grains at the edge of the domains are commonly oblique (up to 10°) as illustrated for the biotite zone in Fig. 3(a). Quartz, within the quartz-rich layers, commonly exhibits undulose extinction and subgrain formation, but many grains are undeformed with regular grain boundaries and 120° triple junctions. Local strain variations at both a meso- and microscopic scale have resulted in the evolution of the crenulation cleavage into a pervasive schistosity (Fig. 3d) (Worley and Wilson, 1996, fig. 6). The local increase in strain is manifest in the garnet-zone samples by an increase in the thickness of the P-domains and a progressive reorientation of Q-domain muscovite into parallelism with the domain boundaries. With increasing strain and temperature (i.e. to the southeast of sample C93/190B), the S_2 fabric has completely recrystallized into a pervasive schistosity defined by the preferred alignment of muscovite. Evidence of the pre-existing crenulation cleavage is only locally preserved in low-strain regions such as porphyroblast pressure shadows,.

The S_2 fabric illustrated in Fig. 3(d–h) is locally deformed by a second, oblique crenulation cleavage (S_{3p}; Worley and Wilson, 1996). Garnet and biotite porphyroblasts overgrow this fabric indicating that peak temperatures outlasted the D_2 event responsible for the formation of the S_2 crenulation cleavage. In fact, throughout the Wenchuan-Maowen shear zone the upper greenschist to amphibolite facies metamorphism extended from syn-D_2 to D_{3p}, with the attainment of peak conditions during D_{3p} (Worley and Wilson, 1996).

AVERAGE PRESSURE–TEMPERATURE CALCULATIONS

To assess the contribution of different deformation mechanisms with increasing metamorphic grade, it is important to quantify the pressure–temperature conditions that prevailed during the tectonic evolution of this pelite–psammopelite sequence. Utilizing the average pressure–temperature approach of Powell and Holland (1994) and the THERMOCALC v 2.4 program (Powell and Holland, 1988), peak pressures and temperatures were calculated for the biotite-zone schists (assemblage: biotite + muscovite + chlorite + plagioclase + quartz) and the garnet-zone schists (assemblage: garnet + biotite + muscovite + chlorite + plagioclase + quartz). An independent set of reactions, and hence pressure and temperature, could not be calculated for the chlorite-zone schist (C93/151) due to the high variance of the

Fig. 3. Cleavage morphology of upper biotite-zone (a–c) and garnet-zone (d–h) schists. (a) Discrete crenulation cleavage in mica-rich schist. (dm) refers to muscovite grains which are slightly oblique to the domain boundaries, but distinctly discordant to grains from the Q-domains. (rm) indicates muscovite grains within Q-domains which are slightly reorientated, with respect to each other, around microfolds. Scale bar = 300 μm. (b) Cleavage-parallel biotite porphyroblast preserving the S_1 fabric in the S_2 Q-domain. Scale bar = 400 μm. (c) Biotite porphyroblast overgrowing and preserving S_2 cleavage domains (S_i). (rm) refers to reoriented muscovites within S_2 Q-domains. Scale bar = 400 μm. (d) Generally discrete cleavage to pervasive schistosity in the mica-rich layer. Large garnet porphyroblast has overgrown a crenulated S_1 fabric but is wrapped by the nearly pervasive S_2 fabric. Scale bar = 1 mm. (e) Asymmetric crenulation cleavage with thick P-domains within the mica-rich schist. Scale bar = 300 μm. (f) Discrete crenulation cleavage in the mica-rich schist. Undulose extinction (und) and subgrain boundaries (sub) are common in quartz grains, muscovite grains are strongly reoriented (rm) around microfold hinges. Scale bar = 300 μm. (g) Biotite porphyroblast in mica-rich schist which has preserved a crenulated S_1 fabric (S_i) and layers of quartz inclusions which are equivalent to the S_2 Q-domains in the matrix. Scale bar = 1 mm. (h) Same biotite porphyroblast as (g), photographed under crossed-nicols to illustrate the preservation of intracrystalline deformation in the form of kink-bands. Scale bar = 1 mm.

assemblage: muscovite + chlorite + albite + quartz. However, an estimated temperature of 380–420°C is based on the apparent metamorphic field gradient and similar reported temperatures for chlorite-zone schists elsewhere (Turner, 1981; Yardley, 1989). Calculated pressures and temperatures for the biotite- and garnet-zone schists, along with 2σ errors and σ_{fit} values, are presented in Table 1. The values of σ_{fit} less than 1.39 indicate that the χ^2 test has been passed at the 95% confidence level and, therefore, that the P–T estimates are consistent with the input data within their uncertainties (Powell and Holland, 1994). Electronic copies of the probe analyses, activities calculated using the program AX (Holland, unpublished 1995) and full THERMOCALC results are available from the first author upon request.

The pressure values range from 500 to 690 MPa (5–6.9 kbar), and are identical within the 2σ uncertainties. Thus, average temperature calculations were performed for each sample at a constant pressure of 600 MPa (Table 1). A result of adopting the average temperature approach is that the calculated temperatures are more tightly constrained than using the average pressure–temperature method. Although the absolute uncertainties are still quite large, the results are strongly correlated because much of the input is common for all samples. Therefore, the relative uncertainties between the biotite- and garnet-zone temperatures are likely to be considerably less than the quoted values (Powell and Holland, 1988). The temperature values for the biotite-zone schists (487 ± 66 and 519 ± 74°C) were obtained using composition data from minerals related to the crenulation cleavage formation and, hence, should provide an indication of the conditions that prevailed during cleavage formation. However, the results from the garnet-zone schists (568 ± 28–584 ± 28°C) were calculated using rim compositions of adjacent garnet and biotite porphyroblasts in apparent equilibrium with the surrounding matrix of muscovite, chlorite, quartz and feldspar, and, hence, should reflect the peak metamorphic conditions. As the metamorphic peak postdates development of the S_2 crenulation cleavage, these results should place an upper constraint of ~580°C on the temperature conditions that prevailed during cleavage formation in the garnet-zone schists.

MINERAL CHEMISTRY

Muscovite from the Q- and P-domains and chlorite from the Q-domains of each sample were analysed with the Cameca Camebax-Microbeam SX-50 electron microprobe housed in the School of Earth Sciences at the University of Melbourne. The aim of analysing the muscovite was to determine whether there is a significant difference between compositions from the different cleavage domains. A difference in composition would indicate that muscovite in the two domains crystallized under different metamorphic conditions, and that 'crystallization equilibration' was the critical equilibration process. Standard operating conditions of a 25 nA beam current, an accelerating voltage of 15 kV and a beam width of 5 μm were used with count times of 10 s for the peaks and 5 s for the background. Mica can be prone to alkali loss during microprobe analysis, but this should be minimized by the beam size and count times. Any loss that is experienced would be consistent for all samples and, therefore, should not affect the following interpretations. The data were reduced using the Cameca PAP matrix correction program (Pouchou and Pichoir, 1984). Representative muscovite analyses are presented in Table 2.

Analyses were collected from P- and Q-domains immediately adjacent to each other, and generally from an area of $< 50\ \mu m^2$ (i.e. Fig. 2b & c, Fig. 3e) to minimize the effect of inherited bulk-rock composition on muscovite composition. Zonal and discrete cleavages from the chlorite-zone sample (C93/151) were analysed, whilst only the domains of discrete cleavages were analysed from the biotite- and garnet-zone schists. Muscovite and chlorite analyses are presented in Figs 4 and 5 where they are plotted on Al_2O_3–$KAlO_2$–(Fe,Mg)O triangular diagrams. This plot is constructed from the AKF and AKM diagrams of Spear (1993) using the recalculated mineral

Table 1. Average P–T results

	Average P–T							Average T at 600 MPa		
Sample	T (°C)	$2\sigma_T$	P (MPa)	$2\sigma_P$	σ_{fit}	ρ_{PT}	No. of independent reactions	T (°C)	$2\sigma_T$	σ_{fit}
Biotite zone										
C93/82	531	114	630	4.6	0.94	0.742	6	519	74	0.8
C93/104	476	108	500	4.4	1.11	0.757	6	487	66	1.0
Garnet zone										
C93/193	579	32	520	1.8	1.08	0.478	9	584	28	1.1
C93/187A	579	30	690	1.6	0.93	0.418	9	571	26	1.0
C93/190B	574	32	650	1.8	1.17	0.445	9	568	28	1.1

$2\sigma_T$ and $2\sigma_P$; 2 standard deviation uncertainties on T and P. ρ_{PT}; correlation coefficient between the uncertainties on P and T.

Table 2. Representative muscovite microprobe data

Sample*	151	151	82	82	104	104	193	187A	190B
Domain	Q	P	Q	P	Q	P	Q	Q	P
Oxides (wt%)									
SiO_2	49.89	47.85	48.28	47.51	47.66	45.58	48.14	48.69	47.50
TiO_2	0.25	0.25	0.25	0.30	0.31	0.30	0.27	0.24	0.28
Al_2O_3	33.32	33.53	34.05	32.95	31.40	30.39	32.25	31.07	33.76
FeO	1.73	1.53	1.94	2.29	1.92	3.37	1.75	2.31	1.87
MgO	1.37	0.96	1.39	1.58	1.78	2.35	1.62	1.92	1.40
MnO	0.00	0.00	0.00	0.00	0.00	0.00	0.07	0.01	0.02
ZnO	0.00	0.00	0.00	0.00	0.00	0.00	0.09	0.00	0.09
CaO	0.00	0.00	0.00	0.02	0.01	0.00	0.00	0.05	0.04
Na_2O	0.41	0.62	0.40	0.40	0.53	0.49	0.71	0.55	0.59
K_2O	8.71	9.57	9.31	9.62	10.15	9.90	10.20	9.92	10.22
P_2O_5	0.00	0.01	0.00	0.00	0.05	0.00	0.03	0.24	0.04
Cl	0.01	0.02	0.01	0.00	0.01	0.01	0.02	0.01	0.00
Cr_2O_3	0.08	0.03	0.00	0.02	0.03	0.01	0.00	0.00	0.06
F	0.16	0.31	0.40	0.22	0.14	0.13	0.14	0.30	0.13
Total	95.95	94.68	96.03	94.93	93.99	92.53	95.29	95.31	96.00
Cations on the basis of 22 oxygens									
Si	6.500	6.367	6.330	6.338	6.435	6.320	6.411	6.477	6.282
Ti	0.024	0.025	0.025	0.030	0.031	0.031	0.027	0.024	0.028
Al	5.116	5.259	5.262	5.181	4.997	4.966	5.062	4.871	5.263
Fe^{2+}	0.188	0.170	0.213	0.255	0.217	0.391	0.195	0.257	0.207
Mg	0.266	0.190	0.272	0.314	0.358	0.486	0.322	0.381	0.276
Mn	0.000	0.000	0.000	0.000	0.000	0.000	0.008	0.001	0.002
Zn	0.000	0.000	0.000	0.000	0.000	0.000	0.009	0.000	0.009
Ca	0.000	0.000	0.000	0.003	0.001	0.000	0.000	0.007	0.006
Na	0.104	0.160	0.102	0.103	0.139	0.132	0.183	0.142	0.151
K	1.448	1.625	1.557	1.637	1.748	1.751	1.733	1.684	1.724
P	0.000	0.001	0.000	0.000	0.006	0.000	0.003	0.027	0.004
Cl	0.002	0.005	0.002	0.000	0.002	0.002	0.005	0.002	0.000
Cr	0.008	0.003	0.000	0.002	0.003	0.001	0.000	0.000	0.006
F	0.066	0.129	0.166	0.093	0.060	0.057	0.059	0.126	0.054
Total	13.723	13.934	13.928	13.957	13.997	14.137	14.017	13.999	14.012

*Sample numbers carry the prefix: C93/.

analyses. Although by grouping Fe and Mg the ability to observe the extent of the $Fe_{-1}Mg$ exchange is lost, the diagram is useful as it enables: (i) chlorite and muscovite to be plotted together; (ii) illustration of the important Tschermak's (Al_{-2}[Fe,Mg]Si) exchange; and (iii) observation of K-deficiency in the 12-coordinated site of muscovite. Deficiency in the 12-coordinated (XII) site of muscovites from metamorphic rocks is a feature common to both microprobe and wet chemical muscovite analyses (Guidotti, 1984), indicating that it is not simply an analytical effect of the microprobe technique (e.g. volatile loss). Figures 4 and 5 show that all of the muscovite analyses from this study are deficient in K relative to pure muscovite–phengite solid solution compositions. To investigate further the nature and significance of this deficiency, all muscovite analyses from the discrete cleavages have been plotted on diagrams constructed to illustrate the (XII)-site deficiency along the y-axis and (Fe + Mg) in excess of the Tschemak's exchange along the x-axis (Fig. 6). Two lines have been drawn on these diagrams: (i) where the (XII)-site deficiency and excess (Fe,Mg) are explained by the substitution $2K(+Na)^{XII} = (Fe,Mg)^{2+} + 2\square^{XII}$ (where $\square$ indicates a vacant site), which is related to deviation of the octahedral sheet from dioctahedral towards trioctahedral (Guidotti, 1984); and (ii) a mixing line between muscovite and chlorite (solid solution of clinochlore and daphnite), as would apply if the electron beam accidently analysed some chlorite with the muscovite. The error bars on these diagrams have been calculated by assuming a 2% analytical error on the most abundant component, i.e. Si and K, on the x- and y-axes, respectively.

Chlorite zone

Muscovite compositions from the Q- and P-domains of both zonal and discrete crenulation cleavages contain significant concentrations of Fe and Mg, but lie off the Tshermak exchange vector in Fig. 4 (Fig. 4a & b). Chlorite contents lie off the Al_2O_3–(FeMg)O side of the diagram, extending toward the muscovite compositions (Q-domain muscovites in the discrete cleavage). Although there is no noticeable compositional difference between muscovites from the Q- and P-domains of the zonal crenulation cleavage (Fig. 4a–l), muscovites from the P-domain of the discrete cleavage are distinctly higher in K relative to those from the Q-domain (Fig. 4a & b). The same distinction can be made in Fig. 6(a) where the Q-domain muscovites, with the lower K contents, have more vacancies. Apart from a number of Q-domain

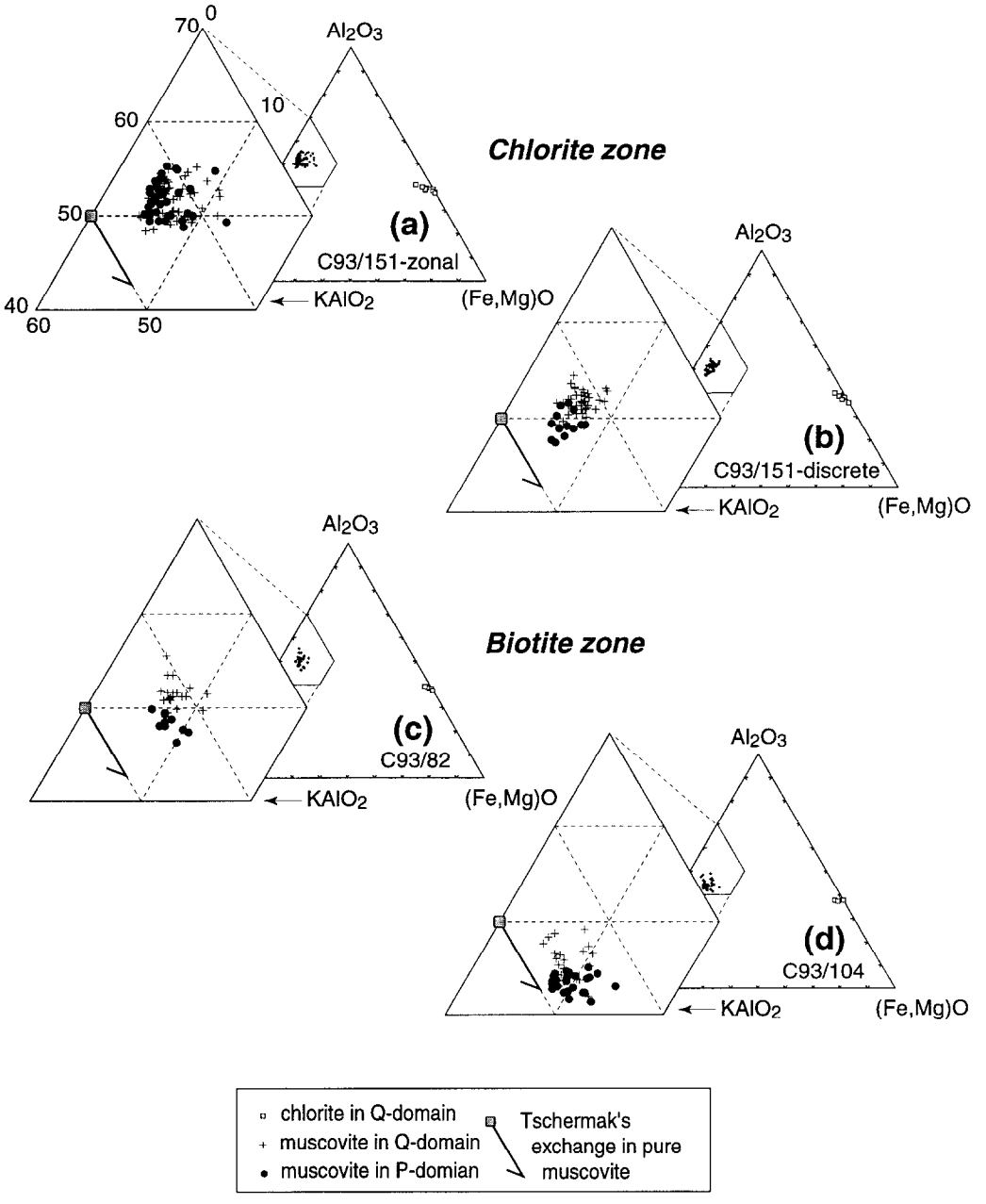

Fig. 4. Al_2O_3–$KAlO_2$–(Fe,Mg)O (AKF-M) diagrams illustrating the range in chlorite and muscovite compositions in chlorite (a & b) and biotite (c & d) zone samples. Apices are calculated from the molecular proportions of the minerals.

analyses, which exhibit a Si excess relative to (Fe + Mg), the muscovites from sample C93/151 lie along the $2K(+Na)^{XII} = (Fe,Mg)^{2+} + 2\square^{XII}$ substitution.

Biotite zone

Muscovite compositions from the lower biotite zone (Fig. 4c) exhibit a similar range to those from the discrete cleavage of the chlorite-zone sample. The P-domain muscovites have slightly higher K- and Tschermak-contents than the Q-domain. The number of vacancies for analyses from each domain are similar and again appear to be explained by the $2K(+Na)^{XII} = (Fe,Mg)^{2+} + 2\square^{XII}$ substitution. Although the Q-domain analyses exhibit a slight spread towards the chlorite–muscovite mixing line in Fig. 6(a), this is not illustrated in Fig. 4(c) where the separation between the two groupings appears to be completely unrelated to chlorite mixing.

Although the K-deficiencies are much smaller than those observed for the chlorite- and other biotite-zone samples, the Q- and P-domain muscovites from the upper biotite zone form two distinct groupings separated along the Tschermak's exchange vector (Fig. 4d). Within these two groups there is considerable scatter towards the chlorite compositions. This feature is also illustrated in Fig. 6(c) where the Fe + Mg in excess of the Tschermak exchange can be explained by mixing with chlorite.

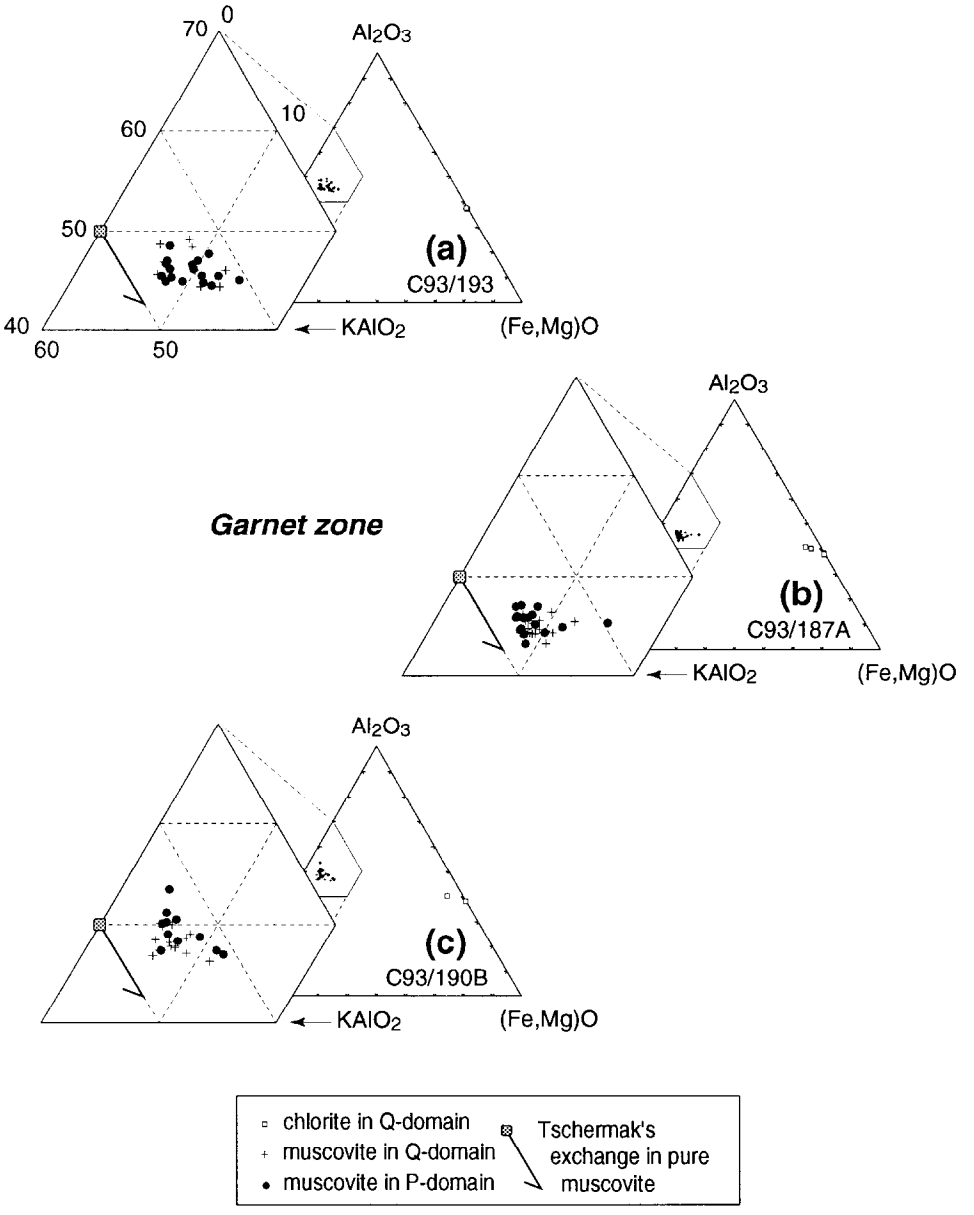

Fig. 5. Al_2O_3–$KAlO_2$–(Fe,Mg)O (AKF-M) diagrams illustrating the range in chlorite and muscovite compositions in garnet-zone samples. Apices are calculated from the molecular proportions of the minerals.

Garnet zone

All three garnet-zone schists exhibit similar variations in muscovite composition with no distinction between muscovite from the Q- and P-domains (Fig. 5a–c). All the analyses, however, exhibit deficiencies in the (XII)-coordinated site and excess Fe + Mg relative to the Tshermak's substitution. As for the upper biotite zone, the compositions scatter towards the chlorite analyses in Fig. 5(a–c) and approach the muscovite–chlorite mixing line in Fig. 6(d–f).

DISCUSSION

The critical microstructural and chemical observations, summarized in Table 3, are discussed in the context of constraining the diffusion, equilibration and deformation mechanisms during crenulation cleavage formation. Observations with increasing metamorphic grade illustrate how the contributions of these mechanisms evolve with increasing temperature.

Zonal vs discrete crenulation cleavage

Although supporting the generally accepted theory that crenulation cleavage formation at low metamorphic grade is related to mass transfer processes (e.g. Cosgrove, 1976; Gray, 1977, 1979; Gray and Durney, 1979; Swager, 1985; Waldron and Sandiford, 1988), the observations presented here illustrate several important details of the mass transfer process, particularly as the development of

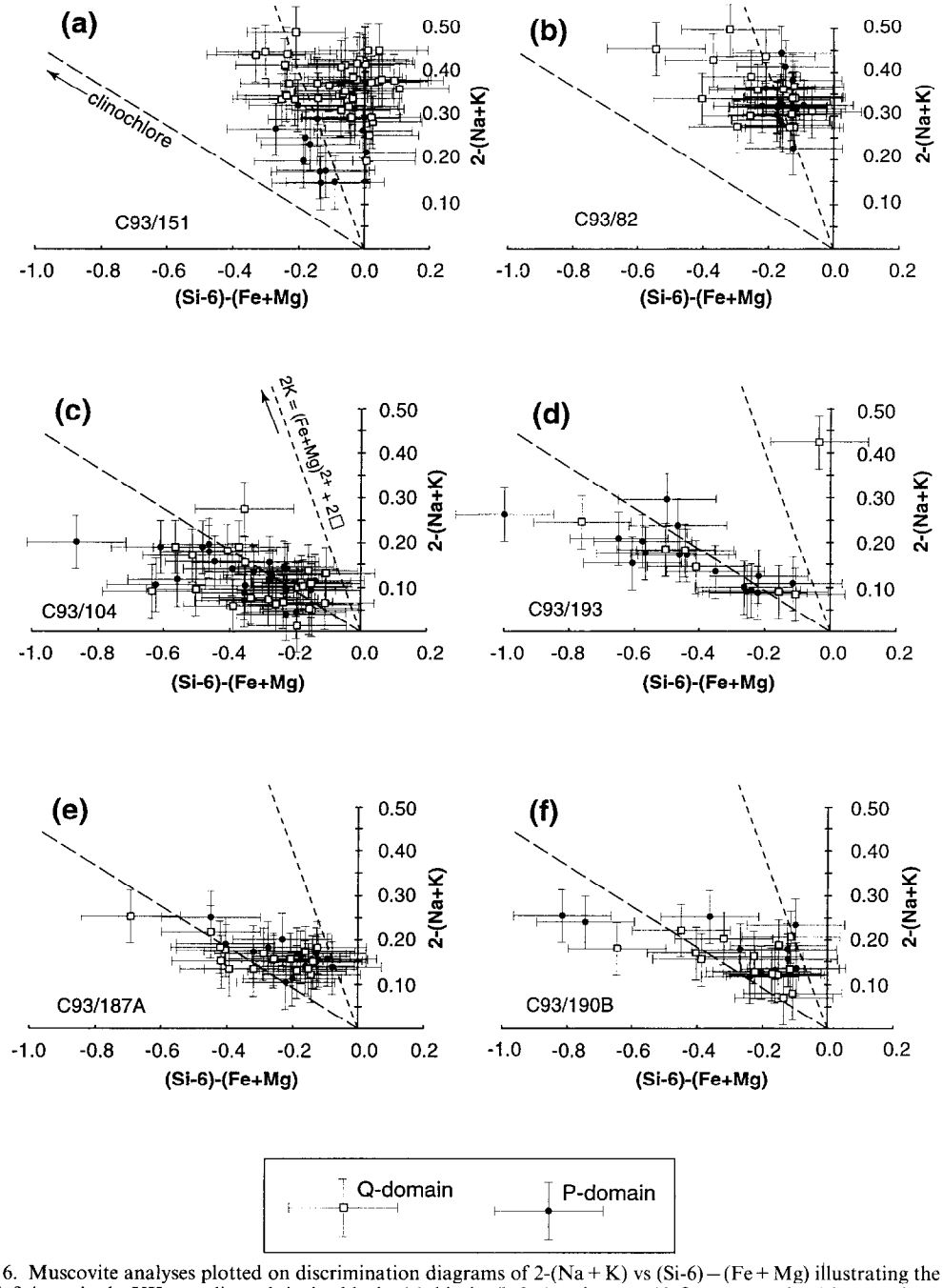

Fig. 6. Muscovite analyses plotted on discrimination diagrams of 2-(Na + K) vs (Si-6) − (Fe + Mg) illustrating the nature of the deficiency in the XII-coordinated site in chlorite (a), biotite (b & c) and garnet (d–f) zone samples. The sample numbers are shown for comparison with Figs 4 and 5. Two trends are illustrated on the diagrams: the long dashed line is a mixing line between muscovite and a solid solution of chlorite and the short dashed line represents the $2K(+Na)^{XII} = (Fe,Mg)^{2+} + 2\square^{XII}$ substitution.

the crenulation cleavage proceeds and a discrete cleavage forms. The development of the zonal crenulation cleavage on the limbs of microcrenulation folds and the similarity of muscovite compositions in both the P- and the Q-domains support a model such as that proposed by Gray and Durney (1979), in which cleavage development is due to a combination of microfolding (mechanical rotation of grains) and stress-driven solution deposition of quartz resulting in the passive concentration and alignment of mica grains in cleavage P-domains. In such a model the mass transfer of material from the limbs to the hinges of the microfolds is considered to be via a grain-boundary fluid. In these examples Gray and Durney (1979) did not consider advective flow of the grain-boundary fluid to be important.

The longitudinal transition of cleavage morphology from zonal to discrete along single cleavage domains illustrates a close relationship between the zonal and discrete cleavage end-members. Although the Gray and Durney (1979) model explains most aspects of the zonal

Table 3. Summary of critical data that relate to crenulation cleavage development

Chlorite zone	Biotite zone	Garnet zone
• Crenulation cleavage morphology evolves from zonal to discrete longitudinally along single domains	• Crenulation cleavage morphologies range from zonal to discrete within individual samples, but there is an increasing dominance of discrete cleavages	• Crenulation cleavage morphologies range from zonal to discrete, but are generally discrete in mica-rich layers
• Zonal and discrete cleavages are closely related to microfolding of the pre-existing fabric	• The first appearance of biotite is as equant porphyroblasts which overgrow S_1 within Q-domains	• Muscovite is highly discordant across microcrenulation hinges
• Extensive thinning and truncation of quartz-rich layers is associated with discrete crenulation cleavage	• In the upper biotite zone, biotite is a major cleavage-forming mineral and locally overgrows the S_2 crenulation cleavage. Biotite porphyroblasts from both the lower and upper biotite zone are undeformed	• The timing of garnet and biotite porphyroblast growth ranges from syn-D_2 to syn-D_3, and early biotite porphyroblasts exhibit intracrystalline deformation in the form of ubiquitous kink-band development
• P-domains of discrete crenulation cleavages are graphite-rich compared with zonal crenulations which are graphite-poor	• Intracrystalline deformation is weak in mica-rich layers, but quartz grains from quartz-rich layers exhibit mild undulose extinction and subgrain formation	• Quartz grains from both mica-rich and quartz-rich layers exhibit undulose extinction and subgrain formation
• Microstructures associated with intracrystalline deformation are absent from mica-rich layers and rare in quartz-rich layers		• Recovery features such as triple junctions with 120° dihedral angles are common in the almost monomineralic quartz-rich layers
• Muscovite compositions from P- and Q-domains of zonal cleavages are indistinguishable and there is a distinct difference in the composition of muscovite from the different domains of discrete cleavages	• There is a distinct compositional difference between muscovite compositions from P- and Q-domains of the discrete crenulation cleavages	• The compositions of muscovite grains from P- and Q-domains are indistinguishable

crenulation cleavage it runs into problems with a number of critical features of the discrete cleavage. The extent of thinning and truncation of quartz-rich layers in the cleavage-affected limbs of F_2 buckle folds (Fig. 2a) cannot be explained simply by diffusive transfer of SiO_2 from the hinge to the limbs of the microcrenulations. These thick discrete cleavage domains appear to represent localized zones of quartz dissolution, and possibly graphite precipitation, but the site(s) of quartz precipitation are not so obvious. The scale and localized nature of the discrete cleavages suggest that transport was not purely by diffusion through a stationary film of grain-boundary fluid, but that the fluid itself was migrating and the discrete cleavages have resulted from localization of the fluid flow during the formation of the buckling instability (Cosgrove, 1976). The discrete cleavages, however, do not appear to form a coherent interconnecting network which would be implied for large-scale advective fluid flow such as that suggested by Etheridge *et al.* (1983). Rather a model in which the scale of flow may be not much larger than the length of individual cleavage domains is proposed. Buoyancy is the most probable driving force and the subvertical orientation of the cleavage domains has enabled them to localize a dispersive intragranular flow. Since the cleavage was nucleated by the buckling instability, it dies out away from the buckled competent layer as does the flow localization and hence flow rate (Fig. 7). A consequence is that the grain-boundary fluid would have been moving during formation of the zonal crenulation cleavage. However, the dispersed grain-boundary fluid may have remained stationary until the vertical cleavage domains reached a critical stage of development at which they were able to trigger and localize buoyancy-driven flow. Once the discrete cleavage developed, with fluid flow focused into it, fluid flow would also occur through the zonal crenulations that terminate the discrete cleavage. The lack of observable deposition sites suggests that the intergranular fluid may continue to migrate via a dispersive flow, until another cleavage network is encounted, resulting in open system behaviour at the scale of the observations. Alternatively, the quartz is crystallized throughout the rock along grain edges away from the ends of the discrete cleavage. Although not observed, the minor dilation implied would be very difficult to see.

'Crystallization' vs 'diffusive' equilibration

Unless the temperature is high enough, so that volume diffusion is significant, equilibration of mineral compositions is controlled by crystallization or recrystallization. The most dominant of the competing intercrystalline transport mechanisms—grain-boundary diffusion or advection—will not explicitly affect the equilibration process, only the scale over which the strain and material can be distributed. Hence, this question cannot be addressed in the following discussion. The importance of 'crystallization equilibration' at chlorite- to biotite-zone conditions ($T < 520$°C) is illustrated by the distinct difference observed in muscovite compositions from the P- and Q-domains of discrete cleavages (Fig. 4b–d). This

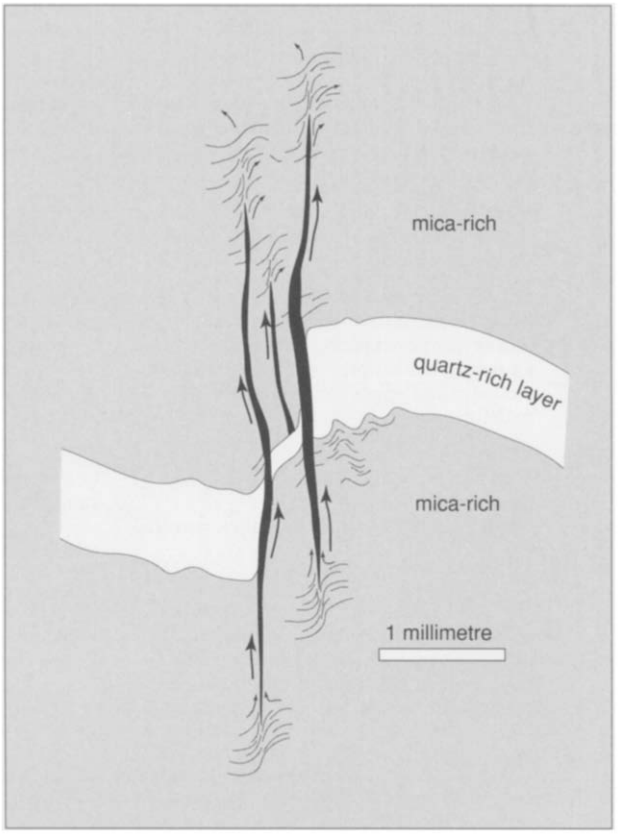

Fig. 7. Schematic sketch of fluid flow patterns associated with discrete crenulation cleavage development.

difference suggests that the strongly aligned muscovite in the P-domains has recrystallized and in doing so equilibrated to the changing chemical and/or pressure–temperature conditions. In the biotite zone, crystallization of biotite is also important to the equilibration and hence deformation process, particularly in the upper biotite zone where biotite is a major cleavage-forming mineral. Having made the observation that volume diffusion is negligible at chlorite- and biotite-zone temperatures, it is likely that the composition of the essentially undeformed Q-domain micas remained unaltered during the cleavage-forming process.

The interpretation of crystallization equilibration in these low-grade samples is supported by the general lack of intracrystalline deformation features as the rearrangement of dislocations through processes, such as climb, to form undulose extinction and subgrain boundaries requires volume diffusion. The preservation of these visible deformation features indicates that volume diffusion was an active process, but complete grain-boundary migration recrystallization, or recovery, was not possible probably due to relatively high strain rates.

The composition of P- and Q-domain muscovite is indistinguishable in garnet-zone schists. This compositional homogenization is unlikely to be the result of complete muscovite recrystallization during the crenulation cleavage formation because, although much of the Q-domain muscovite is deformed, it still defines the crenulated S_1 fabric. Thus, the equivalence in composition suggests that equilibration of muscovite, at temperatures of $\sim$570–590°C, is controlled by volume diffusion, i.e. 'diffusive equilibration'. The common occurrence of intracrystalline deformation features, such as kinking of biotite, undulose extinction in muscovite + quartz and quartz subgrain formation, also indicates that volume diffusion, within mica and quartz (cf. garnet porphyroblasts), was an active process during cleavage formation. The recognition of grain-boundary migration crystallization, coupled with a post-cleavage metamorphic peak, indicates that the intracrystalline deformation may have been more extensive at the time of cleavage formation. Therefore, the processes of volume diffusion and equilibration continued after the formation of the crenulation cleavage.

CONCLUSIONS—A MODEL OF EVOLVING DIFFUSION, DEFORMATION AND EQUILIBRATION MECHANISMS

Based on the microstructural and chemical observations presented here, the following model has been developed to explain the evolution, with increasing metamorphic grade, of diffusion, deformation and equilibration mechanisms which operate during crenulation cleavage formation. It must be stressed that this model has been developed specifically for the rocks observed in the Wenchuan-Maowen shear zone. How-

ever, particular aspects, such as the way in which deformation and equilibration of metamorphic mineral assemblages can be related by considering diffusion, may be widely applicable.

Crenulation cleavage with a zonal morphology initially develops at chlorite zone conditions of ~380–420°C in response to a combination of microfolding and stress-controlled diffusive mass transfer of material via a grain-boundary fluid, which may be accompanied by dispersive buoyancy-driven flow of the grain-boundary fluid. At this stage the scale of transport ranges from single grains up to approximately half the wavelength of the micro-crenulations, although more is possible if there is much fluid flow.

With increasing strain and alignment of muscovite grains within the crenulation cleavage P-domains, the structural anisotropy represented by these domains reaches a critical stage with development of a crenulation cleavage with a discrete morphology. Buoyancy-driven advective flow of the grain-boundary fluid appears to be triggered at this stage. It is localized along the cleavage domains resulting in extensive dissolution of quartz and precipitation of graphite. Crystallization equilibration of P-domain muscovite results in the development of a composition contrast between P- and Q-domain muscovite.

Grain-boundary diffusion and fluid flow along with crystallization equilibration, including biotite crystallization, remain the dominant diffusion/deformation and equilibration processes throughout the chlorite and biotite zones up to temperatures of at least 520°C. The effect of the exponential dependence of volume diffusion on temperature is that in the garnet-zone schists (at temperatures of ~570–580°C) intracrystalline deformation is ubiquitous and correspondingly equilibration becomes diffusive. Grain-boundary migration recrystallization and recovery in the garnet-zone schists is widespread in Barrovian-type upper greenschist to amphibolite facies terrains where the metamorphic peak generally post-dates deformation. This may, in part, account for the paucity of literature relating crenulation cleavage development in such rocks to intracrystalline deformation mechanisms.

Acknowledgements—The field work for this project was funded by the Australian Research Grants Committee and the National Natural Science Foundation of China, and made possible by logistical support from the Chengdu Institute of Technology. During the initial part of this project B. Worley also gratefully acknowledges the financial support of an Australian Postgraduate Research Award. We would like to thank Sally Sutton and Sharon Mosher for their constructive reviews, and James Evans for editorial comments, which greatly improved the final version of this paper.

REFERENCES

Bell, T. H. and Rubenach, M. J. (1983) Sequential porphyroblast growth and crenulation cleavage development during progressive deformation. *Tectonophysics* **92**, 171–194.

Chen, S., Wilson, C. J. L. and Worley, B. A. (1995) Tectonic transition from the Songpan-Garzê Fold Belt to the Sichuan Basin, southwestern China. *Basin Research* **7**, 235–253.

Cosgrove, J. W. (1976) The formation of crenulation cleavage. *Journal of the Geological Society of London* **132**, 155–178.

Etheridge, M. A., Wall, V. J. and Vernon, R. H. (1983) The role of the fluid phase during regional metamorphism and deformation. *Journal of Metamorphic Geology* **1**, 205–226.

Gray, D. R. (1977) Morphological classification of crenulation cleavage. *Journal of Geology* **85**, 229–235.

Gray, D. R. (1979) Microstructure of crenulation cleavages: an indicator of cleavage origin. *American Journal of Science* **279**, 97–128.

Gray, D. R. and Durney, D. W. (1979) Crenulation cleavage differentiation: implications of solution-deposition processes. *Journal of Structural Geology* **1**, 73–80.

Guidotti, C. H. (1984) Micas in metamorphic rocks. In *Micas; Reviews in Mineralogy*, ed. S. W. Bailey, Vol. 13, pp. 357–467. Mineralogical Society of America.

Marlow, P. C. and Etheridge, M. A. (1977) Development of a layered crenulation cleavage in mica schists of the Kanmantoo Group near Macclesfield, South Australia. *Bulletin of the Geological Society of America* **88**, 873–882.

Powell, R. and Holland, T. J. B. (1988) An internally consistent thermodynamic data set with uncertainties and correlations: 3. Applications to geobarometry, worked examples and a computer program. *Journal of Metamorphic Geology* **6**, 173–204.

Powell, R. and Holland, T. J. B. (1994) Optimal geothermometry and geobarometry. *American Mineralogist* **79**, 120–133.

Pouchou, L. and Pichoir, F. (1984) A new model for quantitative X-ray analysis. *Reserche Aerospatiale* **3**, 167–192.

Putnis, A. (1992) *Introduction to Mineral Sciences*. Cambridge University Press, Cambridge.

Spear, F. S. (1993) *Metamorphic Phase Equilibrium and Pressure–Temperature–Time paths*. Mineralogical Society of America Monograph.

Stephens, M. B., Glasson, M. J. and Keays, R. R. (1979) Structural and chemical aspects of metamorphic layering development in metasediments from Clunes, Australia. *American Journal of Science* **279**, 129–160.

Swager, N. (1985) Solution transfer, mechanical rotation and kink-band boundary migration during crenulation-cleavage development. *Journal of Structural Geology* **7**, 421–429.

Turner, F. J. (1981) *Metamorphic Petrology*. McGraw-Hill, New York.

Vernon, R. H. (1976) *Metamorphic Processes*. George Allen and Unwin, London.

Vernon, R. H. (1977) Microfabric of mica aggregates in partly recrystallised biotite. *Contributions to Mineralogy and Petrology* **61**, 175–185.

Waldron, H. M. and Sandiford, M. (1988) Deformation volume and cleavage development in metasedimentary rocks from the Ballarat Slate Belt. *Journal of Structural Geology* **10**, 53–62.

Wilson, C. J. L. (1973) The prograde microfabric in a deformed quartzite sequence, Mt. Isa, Australia. *Tectonophysics* **19**, 39–81.

Wilson, C. J. L. and Bell, I. A. (1979) Deformation of biotite and muscovite: optical microstructure. *Tectonophysics* **58**, 179–200.

Worley, B. A. and Wilson, C. J. L. (1996) Deformation partitioning and foliation reactivation during transpressional orogenesis, an example from the Central Longmen Shan, China. *Journal of Structural Geology* **18**, 395–411.

Yardley, B. W. D. (1989) *An Introduction to Metamorphic Petrology*. Longman Scientific and Technical, Harlow.